JOURNAL OF VIROLOGY, Sept. 2008, p. 8411–8421 Vol. 82, No. 17
0022-538X/08/$08.00+0 doi:10.1128/JVI.00611-08

A Mouse-Passaged Dengue Virus Strain with Reduced Affinity for Heparan Sulfate Causes Severe Disease in Mice by Establishing Increased Systemic Viral Loads▽

Tyler R. Prestwood, Daniil M. Prigozhin, Kristin L. Sharar, Raphaël M. Zellweger, and Sujan Shresta*

Division of Vaccine Discovery, La Jolla Institute for Allergy and Immunology, 9420 Athena Circle, La Jolla, California 92037

Received 19 March 2008/Accepted 5 June 2008

The four serotypes of dengue virus (DENV1 to DENV4) cause extensive morbidity and mortality. A major obstacle to studying disease pathogenesis and developing therapies has been the lack of a small-animal model. We previously reported isolation of a DENV2 strain, obtained by passaging a clinical isolate between mosquito cells and mice, that caused severe DENV disease in mice and contained multiple mutations, including many in domain II of the envelope (E) protein. Here, we describe a recombinant virus, differing from the non-mouse-passaged virus by two mutations in the E protein, that induces vascular leakage and tumor necrosis factor alpha (TNF-α)-mediated lethality, while the non-mouse-passaged virus causes paralysis. This recombinant virus has a weaker affinity for heparan sulfate, resulting in an increased serum half-life, higher systemic viral loads, and high levels of TNF-α in the serum of infected mice. These results exemplify the role of the E protein in modulating virion clearance and connect the effect of clearance on the systemic viral loads responsible for severe disease manifestations.

The four serotypes of dengue virus (DENV1 to DENV4) are the etiologic agents of dengue fever (DF) and dengue hemorrhagic fever/dengue shock syndrome (DHF/DSS). DF is an acute, self-limited febrile illness. The more life-threatening DHF/DSS is characterized by a transient increase in vascular permeability, resulting in the leakage of plasma to the interstitium. DENV is transmitted to humans primarily by the mosquitoes *Aedes aegypti* and *Aedes albopictus*. It belongs to the *Flaviviridae* family and is related to the viruses that cause yellow fever (YFV), hepatitis C, and the West Nile (WNV), Japanese (JEV), and St. Louis encephalitides (5). DENV is an enveloped virus with a single-stranded, 10.7-kb, positive-sense RNA genome that is translated as a single polyprotein and cleaved into three structural proteins (C, prM/M, and E) and seven nonstructural (NS) proteins (NS1, NS2A, NS2B, NS3, NS4A, NS4B, and NS5) by both viral and host proteases. At present, no effective antiviral therapy or vaccine exists. An estimated 2.5 billion people are at risk for DENV infection worldwide, and 50 million new cases of DF, 250,000 to 500,000 cases of DHF/DSS, and 25,000 deaths are reported per year (14, 16).

Despite the significant public health threat posed by DENV, the mechanisms of viral pathogenesis remain unclear. To better understand DENV disease, several mouse models have been developed. Mouse models of DENV infection include (i) intracerebral injection of suckling mice (50); (ii) mouse brain-adapted DENV strains that rapidly induce encephalitis (12); (iii) A/J (20, 51) and AG129 (26, 52) mice that are infected with a high dose of a non-mouse-adapted DENV strain; (iv) chimeric SCID mice that are transplanted with either human peripheral blood mononuclear cells (58); $CD34^+$ cord blood cells (2), erythroleukemic K562 cells (36), or HepG2 hepatocarcinoma cells (1); and (v) chimeric $RAG2^{-/-}$ $\gamma_c{}^{-/-}$ mice transplanted with human fetal liver-derived $CD34^+$ cells (31). In some of these, typical signs of DENV infection in humans, such as thrombocytopenia (2, 20), rash (2), and fever (2, 31), have been observed. However, the dominant clinical phenotype of susceptible mice is paralysis, which is not often seen in human cases.

As a first step toward creating a more relevant small-animal model of DENV infection, we isolated D2S10, a novel DENV2 strain that causes severe disease in AG129 mice, which lack receptors for both alpha/beta interferon (IFN-α/β) and IFN-γ (53). D2S10 was derived by alternately passaging the non-mouse-adapted DENV2 strain PL046 (a Taiwanese human isolate) between mosquito cells and serum of AG129 mice. The parental DENV2 PL046 strain induced paralysis in AG129 mice, while D2S10 was lethal in the absence of paralysis. Rather, the mice had virus in non-neuronal tissues and showed signs of increased vascular permeability. High levels of inflammatory cytokines, including TNF-α, were found in the sera of D2S10- but not PL046-infected AG129 mice, and the treatment of D2S10-infected mice with neutralizing anti-TNF-α antibody prevented both early death and vascular leakage. Therefore, AG129 mice infected with D2S10 exhibit some salient DHF/DSS features, including increased vascular permeability and "cytokine storm".

In the present study, a full-genome-length infectious cDNA clone of PL046 (PL046-IC) was constructed and subsequently used to identify viral determinants present in the D2S10 quasispecies that were responsible for the acute-disease phenotype. Introduction of the N124D and K128E mutations in the envelope (E) protein of PL046-IC was sufficient to recapitulate the D2S10 phenotype in AG129 mice. The mutations resulted in reduced heparan sulfate (HS) binding affinity that led to an increased serum half-life, likely allowing more viral particles to reach and infect visceral organs, ultimately result-

* Corresponding author. Mailing address: Division of Vaccine Discovery, La Jolla Institute for Allergy and Immunology, 9420 Athena Circle, La Jolla, CA 92037. Phone: (858) 752-6944. Fax: (858) 752-6987. E-mail: sujan@liai.org.

▽ Published ahead of print on 18 June 2008.

ing in higher systemic viral loads. These results highlight the relationship between increased viral loads and severity of disease. This model will be useful for studying DENV infection and testing therapeutics.

MATERIALS AND METHODS

Mice. AG129 mice (129/Sv mice lacking IFN-α/β- and IFN-γ receptors), obtained from Herbert W. Virgin (Washington University School of Medicine, St. Louis, MO), were bred and housed under specific-pathogen-free conditions at the La Jolla Institute for Allergy and Immunology (LIAI). All experiments were approved by the Animal Care Committee at the LIAI. Age- and sex-matched mice at 5 to 6 weeks of age were used for all experiments. Virus was injected intravenously via the tail in a volume of 200 μl. For survival studies, mice were sacrificed when moribund or upon initial signs of paralysis.

Cell cultures and viral stocks. C6/36 cells were obtained from the American Type Culture Collection, BHK cells were obtained from Eva Harris (University of California, Berkeley, CA), and K562 erythroleukemia cell lines were a gift from Ted Pierson (Laboratory of Viral Diseases, National Institutes of Health). BHK cells, K562 cells, and C6/36 cells were grown in minimal essential medium-alpha (Invitrogen), RPMI 1640, or Leibovitz's L-15 (Invitrogen), respectively, all supplemented with penicillin, streptomycin, HEPES, and 10% fetal bovine serum (Gemini Bio-Products). C6/36 infection was performed in 5% fetal bovine serum. Cells were grown at 37°C in 5% CO_2 or at 28°C for C6/36 cells. The DENV2 strain PL046 (Taiwanese isolate; C6/36 cell culture adapted) was adapted to C6/36 cells through at least 20 rounds of amplification and obtained from Huan-Yao Lei (National Cheng Kung University, Taiwan). That stock was passaged two times in C6/36 mosquito cells and designated the parental strain used for these studies. D2S10 was isolated from the serum of AG129 mice after 10 passages as previously described (49); virus was amplified twice in C6/36 mosquito cells and used for all experiments of the previous study. Recombinant viral stocks produced from BHK transfections were propagated two times in C6/36 cells and concentrated via ultracentrifugation, and genome equivalents (GE) were quantified by real-time reverse transcription-PCR (RT-PCR).

Generation of infectious cDNA clones. An infectious cDNA clone of PL046 (pPL046-IC) was constructed by cloning three subgenomic fragments (nucleotides 1 to 5056 [F1, SacI/NsiI], nucleotides 4561 to 7592 [F2, NsiI/StuI], and nucleotides 7079 to 10723 [F3, StuI/XbaI]) of PL046 into pCR2.1-Topo vector (Invitrogen), followed by substitution of these fragments into the pD2/IC plasmid, which contained the infectious cDNA clone of DENV2 16681 strain in a modified polylinker site of pBR322 (27). The pD2/IC plasmid, a gift from Richard Kinney (Centers for Disease Control and Prevention, Fort Collins, CO), was obtained from Eva Harris (University of California, Berkeley, CA). RNA was extracted from the parental PL046 stocks with a QIAamp viral RNA minikit (Qiagen), and cDNA fragments were synthesized by using SuperScript III (Invitrogen). The C6/36 cell culture-adapted PL046 stock, obtained from H.-Y. Lei, was passaged twice in C6/36 cells and used for the isolation and generation of cDNAs. Proper integration into pD2/IC and sequence were confirmed by restriction digestion and full-genome sequencing using previously described primers (11). Overlap extension site-directed mutagenesis was performed to generate pE124-IC, pE128-IC, and pE124/128-IC. HB101 (Invitrogen) was used as the host for construction and propagation of cDNA clones. Standard cloning procedures were followed, except that bacteria were propagated at 30°C.

RNA transcription and transfection. Each of the four plasmids (pPL046-IC, pE124-IC, pE128-IC, and pE124/128-IC) was linearized with XbaI and gel purified by using a QIAquick gel extraction kit (Qiagen). Infectious RNA was generated by in vitro transcription with a RiboMax large-scale RNA production system (T7) (Promega) with the following modifications to the manufacturer's protocol: we used 5 mM concentrations of GTP, CTP, and UTP; 1 mM ATP; and 5 mM 7mG(5′)ppp(5′)A cap analog incubated for 4 h at 30°C with the addition of 2 mM ATP after 30 min. Approximately 5 μg of RNA was introduced into 2×10^5 BHK-21 cells via Lipofectamine (Invitrogen)-mediated transfection. At 48 h posttransfection, virus in supernatant was made into viral stocks after centrifugation at 10,000 × *g*. The entire genome of the viral stocks was confirmed by sequencing.

Quantitation of viral loads in mice. Mice were euthanized via isoflurane inhalation, and blood was collected via cardiac puncture. Serum RNA was isolated by using the QIAamp viral RNA minikit (Qiagen). Mice were perfused with 60 to 90 ml of phosphate-buffered saline (PBS), tissues were cut less than 0.5 cm thick in at least one dimension and collected into RNAlater (Qiagen). Bone marrow was taken from the femur, and the peripheral lymph nodes were a pool of the inguinal, brachial, and axillary lymph nodes. Within 24 h, whole tissues were homogenized for 3 to 4 min at 4°C in 1 ml of tissue lysis buffer (Qiagen Buffer RLT) by using a Mini-Beadbeater-8 (BioSpec Products). For small intestine and liver tissues, a fraction of this homogenate was homogenized for an additional minute. Immediately after homogenization, all tissues were centrifuged (5 min, 4°C, 16,000 × *g*) to pellet debris, and RNA was isolated by using an RNeasy minikit (Qiagen). After elution, viral RNA was snap-frozen in liquid N_2 and stored at −80°C until measured by using real-time RT-PCR.

Quantitative RT-PCR. Quantitative RT-PCR was performed according to a published protocol (19), except that a MyiQ single-color real-time PCR detection system (Bio-Rad) with an iScript One-Step RT-PCR kit for Probes (Bio-Rad) were used. The DENV standard curve was generated with serial dilutions of a known concentration of DENV genomic RNA in vitro transcribed (MAXIscript kit; Ambion) from a plasmid containing the cDNA template of PL046 3′-untranslated region. After transcription, DNA was digested with DNase I, and RNA was purified by using an RNeasy minikit (Qiagen) and quantified by UV spectrophotometry. To control for RNA quality and quantity, the level of 18S rRNA was measured by using an 18S rRNA control kit (Eurogentec) in parallel real-time RT-PCRs. A relative 18S standard was made from total splenic RNA. Readings were averaged from duplicates.

Quantitation of vascular permeability. The relative plasma leakage was measured by the concentration of albumin in tissues at day 3 p.i. Mice were euthanized by isoflurane inhalation and perfused with 60 to 90 ml of PBS. Slices of large intestine were collected and homogenized. A capture enzyme-linked immunosorbent assay (ELISA) was performed on homogenates by using a mouse albumin ELISA kit (Bethyl Labs) with the provided absolute standards. Albumin concentrations were measured as milligrams per gram of tissue weight with a limit of detection of 0.74 mg/g.

Measurement and neutralization of TNF-α. TNF-α was quantitated by using a mouse TNF-α ELISA Ready-SET-Go kit (eBioscience) according to the manufacturer's protocol, and results were expressed as picograms per milliliter with a limit of detection of 15 pg/ml of serum. TNF-α was neutralized via intraperitoneal injection of 100 μg of purified, functional-grade anti-mouse TNF-α (clone MP6-XT3; eBioscience) on days 1, 2, and 3 p.i. Purified, functional-grade rat immunoglobulin G1 (eBioscience) was used as the isotype control.

Flow cytometric analysis. Intracellular antigen staining was performed by using the BD Cytofix/Cytoperm kit (BD Biosciences). Cells were labeled with biotinylated anti-DENV prM (clone 2H2) or isotype control anti-colchicine (clone C44), followed by phycoerythrin (PE)-labeled streptavidin (eBioscience). The data were recorded by using a FACSCalibur flow cytometer with CellQuest software (Becton Dickinson) and analyzed by using FlowJo (Tree Star, Inc.).

Infection inhibition with soluble GAG and GAG lyase treatment. The following reagents were obtained from Sigma: heparin (from porcine intestinal mucosa), HS (from bovine kidney), chondroitin sulfate A (from bovine trachea), heparinase I, and chondroitinase ABC. Experiments were performed as previously described (6). Briefly, virus was either preincubated with the specified concentration of soluble GAG for 30 min on ice, or cells were pretreated with GAG lyase at 37°C for 1 h with constant shaking. Cells were washed and then incubated with virus for 1 h at 4°C with constant shaking. Finally, cells were kept on ice and washed extensively by using ice-cold buffer. All incubations were performed in 5 mM $CaCl_2$–5 mM $MgCl_2$–0.5% bovine serum albumin in PBS. RNA from a fraction of the cells was isolated and quantified by quantitative RT-PCR, while the remainder was resuspended in medium and plated in 12-well plates. DENV antigen was detected 24 h p.i. as described above.

Heparin-Sepharose chromatography. Prepacked 1-ml heparin-Sepharose HiTrap HP columns (GE Healthscience) were equilibrated with 5 mM phosphate containing 0.5% bovine serum albumin (pH 7.5). Approximately 10^{10} GE of virus purified over a sucrose gradient, as previously described (17), was applied to the column and then eluted by using a linear gradient from 0 to 500 mM NaCl at a rate of 1.0 ml/min. Then, 1-ml fractions were collected, and virus in fractions was quantitated by real-time RT-PCR.

Statistical analysis. Data were analyzed with Prism software (GraphPad Software, Inc.). For survival studies, Kaplan-Meier survival curves were analyzed by the log-rank test. Statistical significance was determined by using the two-tailed paired *t* test for in vitro experiments and the Mann-Whitney test for mouse experiments, as well as for viral RNA per PFU comparisons.

RESULTS

Initial characterization of recombinant viruses. In our previous study, we reported isolation of D2S10, a mouse-passaged variant derived from the DENV2 strain PL046 that caused severe disease in mice. Eight nucleotide differences between

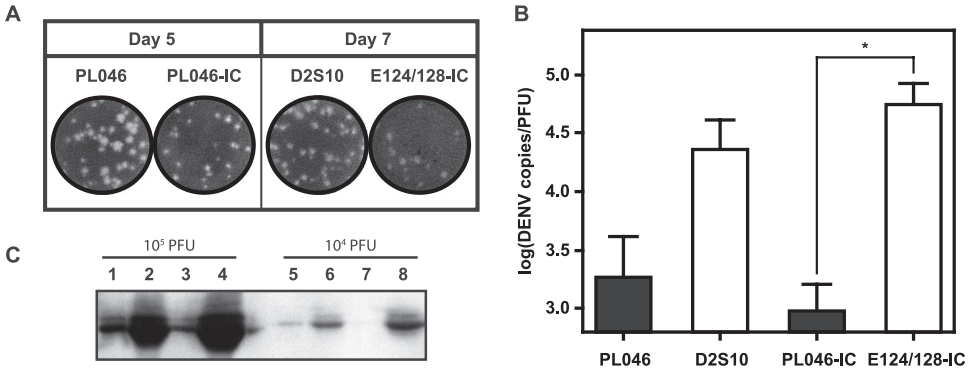

FIG. 1. Comparison of uncloned DENV2 strains PL046 and D2S10 with recombinant viruses derived from pPL046-IC (PL046-IC) and pE124/128-IC (E124/128-IC). (A) Plaque assays using BHK-21 cells were performed. Plaques were visualized day 5 p.i. for PL046 and PL046-IC and day 7 p.i. for D2S10 and E124/128-IC. (B) Virus was quantified by real-time RT-PCR in five different uncloned and four different recombinant preparations. The same preparations were used for plaque assay on BHK-21 cells to calculate viral RNA copies per PFU. The data represent means ± the standard errors of the mean (SEM). The asterisk indicates a difference that is statistically significant ($P < 0.05$). (C) Western blot of uncloned PL046 and D2S10 and recombinant viruses derived from pPL046-IC and pE124/128-IC. A monoclonal antibody (clone E18) was used to detect the E protein in 10^5 PFU of PL046 (lane 1), D2S10 (lane 2), PL046-IC (lane 3), and E124/128-IC (lane 4) and 10^4 PFU of PL046 (lane 5), D2S10 (lane 6), PL046-IC (lane 7), and E124/128-IC (lane 8). In this denaturing gel, the E monomer is detected as the major band of approximately 55 kDa.

PL046 and D2S10 were identified by consensus sequencing (53). One resulted in an amino acid substitution (K to E) at position 128 of the E protein, and another was found in the 3′ untranslated region (T to A; position 10,564), while the remaining mutations were silent. By sequencing individual clones, nine coding mutations were found at amino acid residues 122, 124, 126, 128, 130, 222, 228, and 229 of the E protein, the majority of which resulted in net negative charge changes. To identify viral determinants responsible for the D2S10 phenotype, full-genome-length infectious cDNA clones were generated by reverse genetics. First, an infectious cDNA clone based on the PL046 consensus sequence (pPL046-IC) was assembled, and the recombinant PL046-IC virus caused paralysis in AG129 mice, similarly to uncloned PL046. Next, two mutations in the E protein previously identified in the D2S10 population, K128E and N124D (53), were introduced into pPL046-IC by site-directed mutagenesis to generate the recombinant DENV strain E124/128-IC. D2S10 and E124/128-IC required longer to form visible plaques on BHK monolayers than did PL046 and PL046-IC (Fig. 1A). Real-time RT-PCR demonstrated that uncloned D2S10 and E124/128-IC contained ca. 10- or 50-fold more viral RNA per PFU, respectively, compared to uncloned PL046 or PL046-IC, respectively (Fig. 1B). Western blot of viral stocks using anti-flavivirus E protein confirmed that D2S10 and E124/128-IC contained more antigen per PFU than the parental viruses (Fig. 1C). These results show a higher particle-to-PFU ratio for D2S10 and E124/128-IC viruses than for PL046 and PL046-IC. Thus, all infectious doses in the present study were normalized based on GE.

Two mutations in the E protein are sufficient to recapitulate the TNF-α-induced, early death phenotype in mice. AG129 mice infected with 1.5×10^{11} GE of the double mutant virus, E124/128-IC, succumbed to disease between days 3 and 4 p.i. (Fig. 2A), mirroring the published data obtained from studies with D2S10 (53), while AG129 mice infected with the parental PL046-IC virus began exhibiting paralysis by day 12 p.i. Mice infected with virus containing either the N124D or the K128E amino acid change alone manifested paralysis between days 6 and 30 p.i. (data not shown). Since the presence of only one mutation did not cause the early death observed in mice infected with the double mutant, neither vascular leakage nor TNF-α in the serum were measured. The results of survival studies indicate that the presence of both the N124D and the K128E substitutions together is sufficient to recapitulate D2S10 phenotype. To confirm this, vascular leakage and TNF-α levels were assessed in mice infected with E124/128-IC. Similar to mice infected with D2S10 (53), mice infected with E124/128-IC exhibited increased vascular permeability at day 3 p.i., as measured by elevated levels of albumin in the large intestine (Fig. 2B), and contained significantly more TNF-α in the serum than PL046-IC-infected mice (Fig. 2C). In addition, as observed with D2S10, administration of TNF-α-neutralizing antibody prevented the severe disease manifestations (Fig. 2D). Thus, the phenotypes caused by PL046-IC and E124/128-IC are identical to those of mice infected with PL046 and D2S10, respectively.

Reduced infectivity of E124/128-IC on BHK cells. To investigate the differential BHK plaque phenotype, we performed intracellular antigen staining to detect infection of these cells. At inocula of 5,000 GE per cell, higher percentages of the cells infected with PL046-IC were DENV positive than those infected with E124/128-IC at both 24 h and 48 h p.i. (Fig. 3A). The percentage of PL046-IC-infected cells declined from 42.1% at 24 h p.i. to 29.7% at 48 h p.i., most likely due to cytopathic effects of the virus. These results demonstrate that the N124D and K128E mutations decrease the infectivity of BHK cells. K562/DC-SIGN cells are the human erythroleukemic cell line K562 overexpressing DC-SIGN, and these cells, but not wild-type K562 cells, are highly permissive to DENV infection (10). At inocula of 5,000 or 500 GE per cell, the two amino acid changes enhanced the infection of K562/DC-SIGN cells (Fig. 3B). This confirmed that the reduced ability of

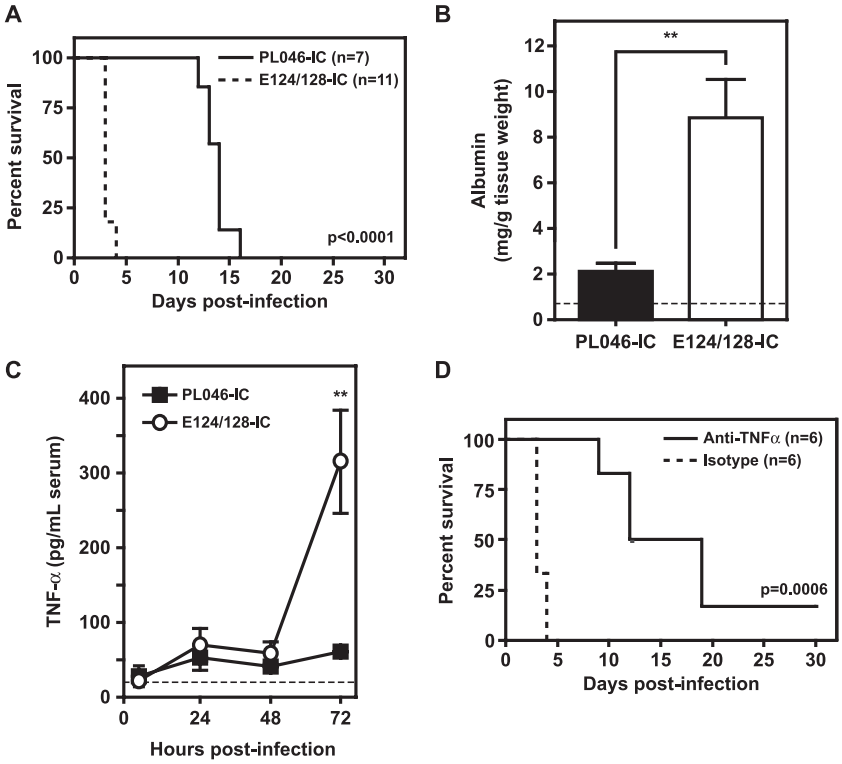

FIG. 2. Infection of IFN-α/β and IFN-γ receptor-deficient 129/Sv (AG129) mice with recombinant DENV2 PL046-IC or E124/128-IC. (A) Survival curves of AG129 mice infected with 1.5×10^{11} GE of PL046-IC or E124/128-IC. All PL046-IC-challenged mice developed paralysis, whereas all E124/128-IC mice died without manifesting paralysis. The *P* value between the two viral strains is indicated. The data from three independent experiments, each with different viral preparations, were pooled (n = the total number of mice per group). (B) Vascular permeability was assessed by measuring albumin concentrations in the large intestine of mice day 3 p.i. by ELISA. The results represent the mean values ± the SEM of five mice per group, except for the naive group with three mice. The dotted line shows the limit of detection of the assay. **, $P < 0.01$. (C) TNF-α levels in the serum were analyzed by ELISA. Mean values ± the SEM of six to nine mice per group for each time point are shown. The dotted line represents the limit of detection of the assay. **, $P < 0.01$. (D) Anti-TNF-α or isotype control antibody was administered to E124/128-IC-infected mice on days 1, 2, and 3 p.i. Isotype control-treated mice succumbed to infection without exhibiting signs of paralysis, whereas anti-TNF-α-treated mice developed paralysis. The data were pooled from two experiments (n = the total number of mice per group; the *P* value is indicated).

E124/128-IC to infect BHK cells was not due to the presence of more defective particles per GE.

HS proteoglycan-dependent infection of BHK-21 cells by PL046-IC and E124/128-IC. Infection of BHK cells by DENV2 has previously been shown to be dependent on HS-mediated viral entry (22, 34). Based on the published DENV2 E protein structure, the amino acids at positions 124 and 128 of E protein in PL046 form part of a basic patch on the external surface of the protein at the base of domain II, near the region postulated to affect receptor interaction (39, 41) (Fig. 4). Positively charged residues in this region of the envelope are present in other DENV2 strains and are speculated to bind HS proteoglycans (40). Since these residues were replaced with negatively charged amino acids in E124/128-IC, we hypothesized that the mutations affected interactions with HS moieties on BHK cells.

Binding assays were performed with BHK cells that were pretreated with heparinase I, which specifically removes cell surface HS. Heparinase I treatment reduced binding of both viral strains to BHK cells (Fig. 5A), confirming that attachment to these cells by both strains is dependent on interactions with HS. Fivefold more PL046-IC bound to untreated BHK cells than E124/128-IC, suggesting that PL046-IC interacts with HS moieties on BHK cells more strongly than E124/128-IC. Next, cells were pretreated with heparinase I or chondroitinase ABC, and the level of infection at 24 h p.i. was assessed by flow cytometry. Heparinase I decreased infection by both viruses (Fig. 5B) and, compared to E124/128-IC, more heparinase I was required to reduce PL046-IC infection to ca. 40% of the untreated control. Neither virus showed reduced infectivity on cells treated with chondroitinase ABC, which specifically degrades cell surface chondroitin sulfate, demonstrating the specificity of interactions between these viruses and HS. Next, infection inhibition assays with soluble heparin, HS, or chondroitin sulfate A were performed. HS is widely expressed on the surface of cells and extracellular matrices at degrees of sulfation that vary based on the organ. Heparin is a highly sulfated species of HS, while the HS used in this experiment is less sulfated. Thus, heparin and HS are used experimentally to test the importance of sulfation for interactions with the virus, while chondroitin sulfate A is used as a control against nonspecific interactions. Preincubation with heparin substantially decreased both PL046-IC and E124/128-IC infection of BHK cells in a dose-dependent manner (Fig. 5C), although a higher

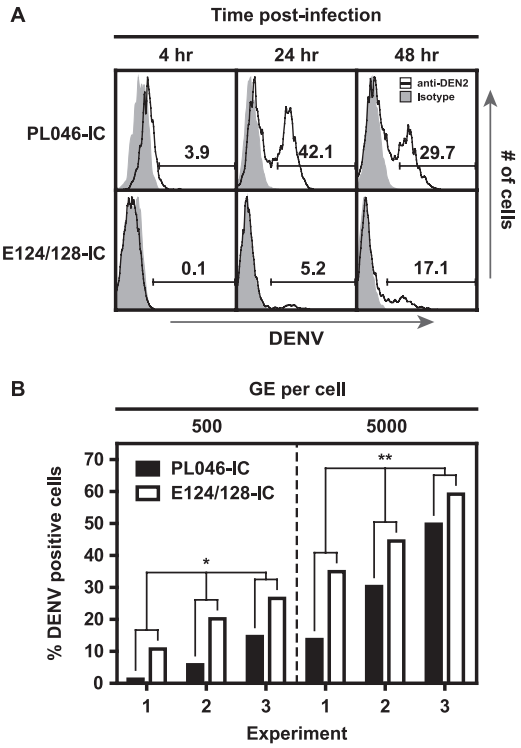

FIG. 3. Infection of BHK and K562 cells by the recombinant viral strains. (A) BHK-21 cells were infected with 5,000 GE of PL046-IC or E124/128-IC, and the presence of DENV prM was detected by flow cytometry. The percentages of positive cells are shown. The data from one representative out of five independent experiments using different viral preparations are shown. (B) K562/DC-SIGN cells were infected with 5,000 or 500 GE of PL046-IC or E124/128-IC, incubated for 24 h, and analyzed by flow cytometry. The percentages of DENV antigen positive cells are shown from three independent experiments with different viral preparations and asterisks denote statistical significance (*, $P < 0.05$; **, $P < 0.01$).

concentration of heparin was required to reduce infection by PL046-IC than by E124/128-IC. In contrast to heparin, HS inhibited infection only at a high concentration (100 μg/ml), and chondroitin sulfate A had no effect. Taken together, these results confirm that infection of BHK cells by either viral strain is strongly dependent on interactions with more sulfated forms of HS. In addition, they suggest that PL046-IC has a greater affinity for binding to heparin than E124/128-IC.

E124/128-IC shows reduced interaction with HS. To test the relative binding affinity of the two DENV strains, sucrose-gradient-purified preparations were examined by heparin-Sepharose chromatography. In agreement with BHK binding and infection experiments, E124/128-IC eluted at a much lower NaCl concentration than PL046-IC, indicating weaker binding of E124/128-IC to heparin (Fig. 5D) and confirming that the N124D and K128E mutations reduce binding affinity to heparin-like forms of HS.

Although PL046-IC binds more strongly to heparin compared to E124/128-IC, binding of both viruses to BHK cells is highly dependent upon interactions with HS. When HS molecules are enzymatically cleaved, their cell surface concentration is reduced. Likewise, in the presence of soluble GAG, HS binding sites on the virus are blocked, and the free binding site

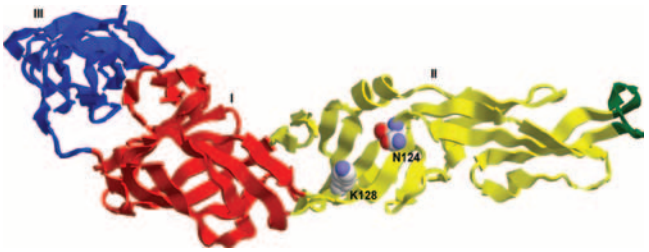

FIG. 4. Localization of K128 and N124E mutations in three-dimensional structure of PL046 E. Positions of N124 and K128 are viewed from the top of the E monomer structure with domain I (red), domain II (yellow), domain III (blue), and fusion peptide (green) based on the published coordinates (39).

concentration is therefore reduced. In both cases, because PL046-IC has a higher affinity for HS, the measured virus-HS interaction is less affected by reduced concentrations of HS or HS binding sites. On the other hand, because E124/128-IC has a lower affinity for HS, its binding is more readily affected.

Virion clearance from the circulation. Previous studies with high-affinity heparin-binding variants of DENV and encephalitic flaviviruses, such as JEV, WNV, and MVE, have shown that mutations in the E protein resulting in gain-of-positive charge translate to rapid virion removal from circulation (32–34). Therefore, we examined whether the gain-of-negative-charge mutations in E protein of E124/128-IC reduce the rate of virion clearance from the blood. A total of 1.5×10^{11} GE of PL046-IC and E124/128-IC was intravenously administered to mice, followed by harvest of serum samples at 0.5, 1.5, and 3 h p.i., and viral RNA was quantified by real-time RT-PCR. At 0.5 h, viral RNA levels were similar between PL046-IC- and E124/128-IC-infected mice (Fig. 6). However, by 1.5 h p.i., serum viral RNA levels in E124/128-IC-injected mice were fivefold higher than in PL046-IC-inoculated mice. By 3 h p.i., ~15-fold more viral RNA was present in the serum of E124/128-IC-infected mice than in PL046-IC-infected mice. The levels of viral RNA decreased in other tissues (lymph nodes, liver, spleen, kidney, and intestine) between 0.5 and 3 h in all animals (Fig. 7), suggesting that the first round of replication was not yet complete. This implies that only input virus was present in the serum at this time. These results demonstrate a longer serum half-life of E124/128-IC relative to PL046-IC.

Kinetics analysis of viral distribution in PL046-IC- and E124/128-IC-infected mice. To investigate whether the extended serum half-life of E124/128-IC was leading to severe dengue disease manifestations in mice, kinetics analysis of viral RNA in tissues between 0.5 and 72 h p.i. was performed. RNA was isolated from serum or tissues of mice infected with 1.5×10^{11} GE of PL046-IC or E124/128-IC, and the levels of viral RNA were quantified by real-time RT-PCR. In the serum, viremia decreased between 0.5 and 3 h, as shown in Fig. 6, but by 7 h p.i. viremia had significantly increased with both viruses (Fig. 7A). The 15-fold difference in viremia between PL046-IC- and E124/128-IC-infected mice at 3 h p.i. increased to ~50-fold by 72 h p.i. In the first 5 h p.i., the viral loads in other tissues were not statistically different between the two viruses and decreased logarithmically. No statistically significant differences in viral loads in the liver, spleen, lungs, and kidneys were observed until 72 h p.i. At this time point, the viral load

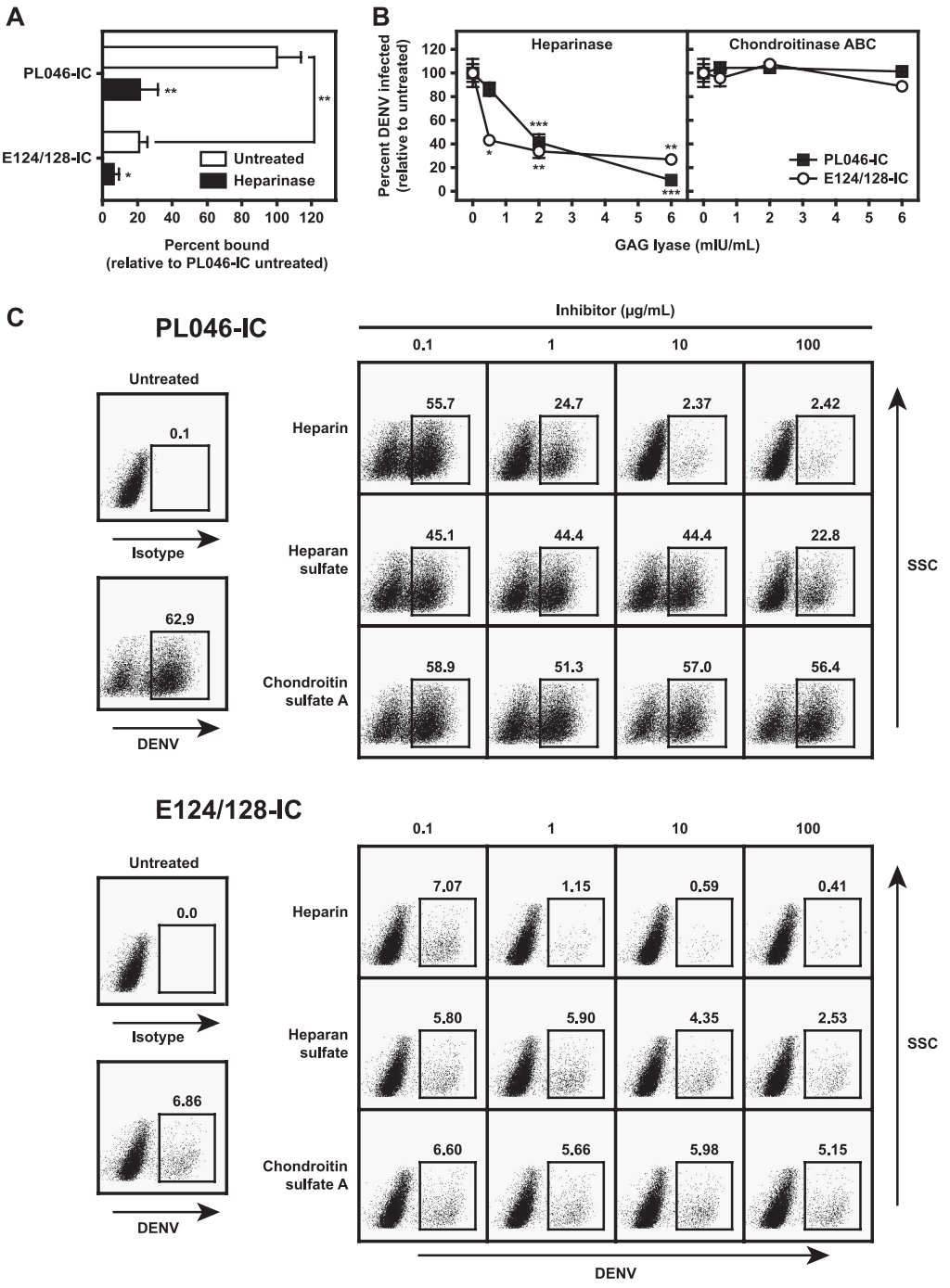

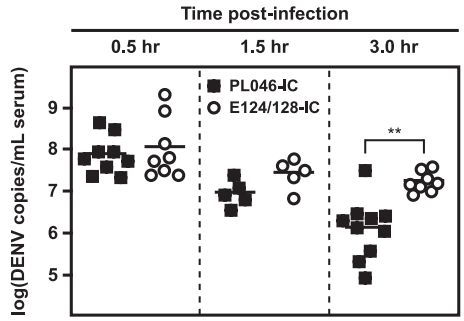

FIG. 6. Clearance of the recombinant DENV virions from circulation. AG129 mice were intravenously infected with 1.5×10^{11} GE of PL046-IC or E124/128-IC. Serum was collected at various time points p.i., and viral RNA levels were quantified by real-time RT-PCR. The data are expressed as GE of DENV RNA per ml of serum. Each symbol represents an individual mouse. Asterisks denote viral RNA levels that are statistically different between PL046-IC- and E124/128-IC-injected mice at 3 h p.i. (**, $P < 0.01$).

in E124/128-IC-infected mice was higher by ~4-fold in the liver, 10-fold in the spleen, 20-fold in the lungs, and 30-fold in the kidneys compared to PL046-IC-infected mice (Fig. 7B). In the bone marrow, peripheral lymph nodes, and mesenteric lymph nodes, higher viral loads were detected at 12 h and 24 h p.i. in E124/128-IC-infected mice than in PL046-IC-infected mice, although the difference in the bone marrow was not statistically significant (Fig. 7C). By 72 h p.i., these tissues contained similar amounts of viral RNA in both PL046-IC- and E124/128-IC-infected mice. In addition to lymph nodes and the bone marrow, the gastrointestinal organs contained the earliest differences between PL046-IC- and E124/128-IC-infected mice. Beginning 12 h p.i., the small intestine of mice infected with E124/128-IC contained significantly higher concentrations of viral RNA than did PL046-IC-infected mice. The large intestine and stomach were also consistently higher, but the differences were not statistically significant (Fig. 7D). These trends continued throughout the infection, remaining 10-fold higher in mice infected with E124/128-IC through 72 h p.i. Collectively, these results show that, relative to PL046-IC, E124/128-IC maintains 15- to 50-fold-higher viremia and establishes ca. 10-fold-higher viral loads in multiple tissues.

To verify that the increased viral loads were responsible for severe disease in mice infected with E124/128-IC, AG129 mice were infected intravenously with 3.0×10^{12} GE of PL046-IC. This dose was chosen to account for the serum difference observed at 3 h p.i. These mice began showing signs of illness less than 24 h before death, and three out of four mice succumbed by 3 to 4 days p.i., while the fourth mouse developed paralysis on day 7 p.i. (data not shown). These results underscore the importance of virion clearance and initial viral loads in establishing the systemic infection responsible for severe disease, as well as confirm that this early death phenotype is due to factors common to both viruses.

DISCUSSION

D2S10 was obtained by passaging PL046, a Taiwanese cell culture-adapted isolate, between C6/36 cells and mice, and it was shown to cause severe dengue disease in AG129 mice. In the present study, we identified mutations present in the D2S10 population responsible for increased virulence in AG129 mice as indicated by the 20-fold-higher dose of the parental virus required to induce severe disease. We suggest that the mechanism of this increased virulence is due to reduced interactions with HS, giving the virus a greater serum half-life and, in turn, allowing more viral particles to reach and infect their targets.

In the present study, we found that E124/128-IC and PL046-IC differ in ability to form plaques on BHK cells, and thus it was not possible to use plaque assays to compare quantities of the virus. In addition, assays that rely on viral particle functionality, such as plaque assay and fluorescence-activated cell sorting-based titration, to measure viral loads are more susceptible to bias due to interactions between tissue homogenates and cells, as well as other factors such as virus inactivation during tissue disruption. For these reasons, real-time RT-PCR provided a means to reduce bias and increase sensitivity when detecting virus in organ homogenates. However, quantifying virus by GE does not discriminate between viral replication and trafficking, nor does it discriminate between infectious particles, defective particles, and nascent RNA. Thus, we cannot definitively conclude in which tissues the virus is replicating. Still, the numerous time points and tissues examined provide the framework for more detailed studies by revealing spatial and temporal sites of importance. To identify actual sites of DENV replication in vivo, the presence of structural and nonstructural viral antigens, as well as negative- and

FIG. 5. Interaction between the recombinant DENV strains and HS proteoglycans. (A) Inhibition of viral attachment to BHK-21 cells by heparinase. BHK-21 cells were pretreated or not with heparinase I, exposed to 5,000 GE per cell of virus for 1 h at 4°C, washed at 4°C, and homogenized, and RNA was isolated. The quantity of DENV present was determined by real-time RT-PCR. The results are expressed as percentages of DENV particles bound to cells relative to the number bound to untreated PL046-IC-infected cells. Error bars represent the SEM of two independent experiments using a total of five or six different viral preparations of E124/128-IC or PL046-IC, respectively. (B) Inhibition of BHK-21 infectivity by heparinase. BHK-21 cells were pretreated or not with heparinase I or chondroitinase ABC, exposed to 5,000 GE per cell of virus for 1 h at 4°C, washed at 4°C, plated, and incubated at 37°C. At 24 h p.i., the presence of DENV prM was detected via flow cytometry. The results are shown as percentages of DENV-positive cells relative to the untreated control. Error bars indicate the SEM corresponding to three independent experiments using four or six different viral preparations of E124/128-IC or PL046-IC, respectively. (C) Inhibition of BHK-21 infectivity with soluble GAG. A total of 5,000 GE per cell of PL046-IC or E124/128-IC was mixed at different concentrations of the indicated soluble GAG prior to incubation with BHK-21 cells for 24 h at 37°C, followed by detection of DENV infection via flow cytometry. Data from one representative out of three independent experiments using eight different viral preparations are shown. (D) Viral binding to heparin. Approximately 10^{10} GE of sucrose-gradient-purified virus was added to heparin-Sepharose columns equilibrated with a phosphate buffer. After a washing step, bound virus was eluted with an increasing NaCl concentration, ranging from 0 to 500 mM. Viral RNA in each fraction was then quantified by real-time RT-PCR. Asterisks denote statistical significance of results (*, $P < 0.05$; **, $P < 0.01$; ***, $P < 0.001$).

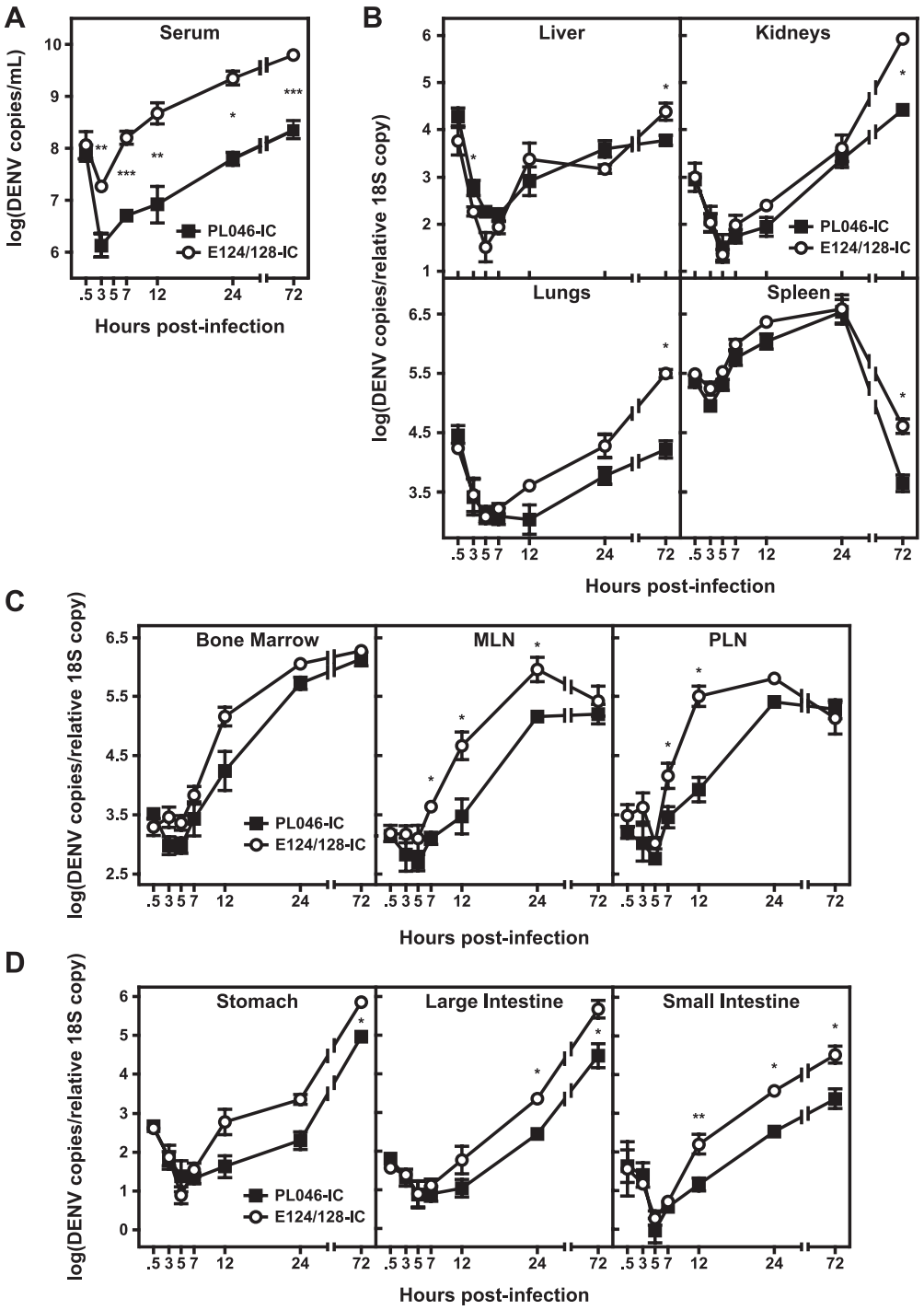

FIG. 7. Levels of viral RNA in tissues of PL046-IC or E124/128-IC-infected mice. (A) Serum; (B) liver, kidneys, lungs, and spleen; (C) bone marrow, mesenteric lymph nodes (MLN), and peripheral lymph nodes (PLN); (D) stomach, large intestine, and small intestine. AG129 mice were intravenously infected with 1.5×10^{11} GE of PL046-IC or E124/128-IC. The indicated tissues were harvested at 0.5, 3, 5, 7, 12, 24, and 72 h p.i., and viral RNA was quantified by real-time RT-PCR. The data are expressed as the geometric mean of DENV RNA copies relative to 18S of 3 to 10 mice per group for each time point. Asterisks denote viral RNA levels that are statistically different between PL046-IC- and E124/128-IC-infected mice (*, $P < 0.05$; **, $P < 0.01$; ***, $P < 0.001$).

positive-strand viral RNA, will be further investigated in tissues identified to be important by the present study.

The two E-protein mutations discussed in the present study, N124D and K128E, occur in a positively charged patch consisting of several other lysine residues postulated to interact with HS (40). Studies with several flaviviruses, including DENV, JEV, WNV, and MVE (32–34), and other viruses, such as foot-and-mouth disease virus (49), Sindbis virus (7, 30),

Venezuelan equine encephalitis virus (3), and classical swine fever virus (55), have shown that adaptation of the virus to growth in tissue culture cells results in gain-of-positive charge mutations in the envelope proteins, thereby promoting viral binding to GAG and this leads to increased viral uptake into cells. Although enhanced GAG binding confers a selective growth advantage in tissue culture, it translates to attenuation in vivo, as the rate of virion clearance from serum is increased. In addition to increased virion clearance, other groups have reported that high-affinity GAG-binding variants demonstrate increased neurovirulence (25, 45, 47). This has been shown with the DENV2 strain PUO-218, as passaging in either mouse brain or BHK cell culture selected for a lysine residue at amino acid 126 of the envelope (34). Amino acids E124 and E128 are located in the same basic patch as E126, and the viruses used in our study share this Lys^{126} residue. Interestingly, Lee et al. (34) found that this Lys^{126} residue was responsible not only for increased HS binding but also for reduced viscerotropism and enhanced neurovirulence. This suggests that HS binding in this region could be contributing to the paralytic phenotype we observed in AG129 mice infected with PL046-IC. The mutations reported here are the opposite charge change, from positive or neutral to negative, of those that arose during mouse brain or BHK cell adaptation, from negative to positive, as reported by Lee et al. (34), and have the opposite function since they result in reduced heparin binding affinity and higher viral replication in non-neuronal tissues in vivo. Thus, the alternate passaging strategy selected for species more fit for replication in non-neuronal tissues, and potentially as a consequence, reduced neurovirulence. In addition, the infectivity of E124/128-IC was increased relative to PL046-IC on K562/DC-SIGN cells when the infectious dose was normalized based on GE. This result may be due to these mutations allowing the formation of more functional viral particles per GE, since the infectious dose for these experiments was not normalized based on viral particle functionality, or due to an increased ability to interact with the DC-SIGN molecule, which has been identified as a DENV attachment receptor on primary human dendritic cells (42, 54). Although the K562/DC-SIGN cells express human DC-SIGN, selection for this may have occurred on a murine homologue during passaging. Nevertheless, we do not believe that this increased infectivity alone could account for the severe disease phenotype in mice, given the magnitude of the differences in viral loads and the 20-fold-higher dose of PL046-IC required to consistently induce the severe disease phenotype.

Studies in human populations have furnished important information about DENV pathogenesis and immunity, but lack of an adequate small-animal model has hampered mechanistic insight into DENV infections. In humans, higher viremia is a defining feature of DHF/DSS compared to DF (35, 56, 57). In particular, DHF/DSS is associated with viremia that is 10- to 100-fold higher in titer than that of DF cases (4). Our findings mirror this observation since infection with E124/128-IC resulted in much higher viremia, ranging from 15- to 50-fold, beginning 3 h p.i. In addition to higher viremia, TNF-α is found more frequently and at higher levels in the plasma of individuals with DHF/DSS than with DF, and an increase in TNF-α levels correlates with increased disease severity (13, 18, 28). In agreement with this, substantial levels of TNF-α were detected in the serum of E124/128-IC-infected but not PL046-IC-infected mice. Elevated levels of this cytokine were present only on day 3 p.i., close to the time of death. Collectively, our studies with mice infected with E124/128-IC support a model of DENV pathogenesis in which high levels of virus in tissues trigger an excessive TNF-α-dependent inflammatory response that quickly leads to vascular leakage and death. Similarly, studies with Sindbis virus have shown that low-affinity GAG-binding variants are able to induce systemic inflammatory response with elevated levels of TNF-α (29, 48). Future studies will attempt to delineate the mechanisms by which viral load, TNF-α, and severity of disease are connected. Whether higher viremia in humans is due to infection with viral strains that behave more like E124/128-IC or to host factors or to both remains to be answered.

Our studies also demonstrate the importance of initial viral concentration in the serum during the early hours after infection. We found that a reduced rate of virion clearance from the serum resulted in increased systemic infection. This differential rate clearance of E124/128-IC and PL046-IC was likely to be mediated by the liver, as shown with other viruses (7, 23), and is exemplified by the presence of more viral RNA in the liver of mice infected with PL046-IC at 0.5, 3, and 5 h p.i., although only the 3-h difference was statistically significant. Liver HS has been shown to be highly sulfated and heparin-like in structure (37), and PL046-IC interacted with heparin more strongly than E124/128-IC in vitro. We speculate that the reduction in strength of interactions with HS is responsible for the reduced rate of virion clearance of E124/128-IC and that this allows a greater number of viral particles to reach cellular targets for replication before destruction in the liver, allowing a greater systemic infection. The effect of this differential virion clearance is first observed at 7 h p.i.; the difference becomes more apparent by 12 h p.i. and is especially pronounced in the lymph nodes and bone marrow. This suggests that these organs are likely early sites of viral replication or trafficking. However, by 24 h p.i., the amount of viral RNA in these organs remains constant or begins to decrease. The amounts of viral RNA in the lungs, kidneys, stomach, small intestine, and large intestine increase from 12 to 72 h, and therefore these organs are probably later sites of replication, since it is unlikely that trafficking alone could account for these observed increases in viral RNA. In these tissues, although more E124/128-IC is present initially, the levels of viral RNA in mice infected with either virus show the same rate of logarithmic increase, implying that once infection in these tissues is established, the viruses replicate and spread at the same rate. Since these mice lack both type I and type II interferon receptors, undoubtedly more viral replication occurs than in immunocompetent mice. However, the present study suggests that DENV replication occurs throughout the visceral organs, and this correlates with human studies in which DENV antigen and RNA have been detected in the serum, liver, spleen, heart, lungs, lymph nodes, and bone marrow (8, 9, 15, 21, 24, 43, 46) and the central nervous system postmortem (38, 44).

Interactions with HS are thought to concentrate HS-binding proteins near the surface of the cells and increase the likelihood of interaction with receptors. The fact that E124/128-IC shows reduced, but not completely disrupted, interactions with HS suggests that either the virus has not been passaged enough

to completely abrogate this interaction or that some interaction with HS is beneficial for the virus in vivo and will be maintained through passaging. If the latter is true, it is likely that interactions with HS in vivo require balance: virus that interacts too strongly is quickly removed from the serum and not given enough time to reach its targets, while virus that interacts too weakly may not get enough of an opportunity to interact with cell surface receptors. Although virion clearance was delayed in mice infected with E124/128-IC, compared to mice infected with PL046-IC, viral RNA in the sera of mice infected with either virus increased by 7 h p.i., implying that the first round of viral replication had completed and took approximately the same amount of time. This indicates that the reduced interactions with HS of E124/128-IC did not detectably compromise its ability to infect initial targets. The importance of this interaction in vivo could be assessed by additional passaging of the virus that would eventually lead to disruption of other HS binding sites, resulting in a loss of interaction with HS, or to maintenance and possibly further optimization of HS binding, demonstrating its necessity. The fact that mutations opposite those seen in the D2S10 population occurred when passaging in either BHK cell culture or mouse brains confirms the validity of passaging virus between mosquito cells and mice to generate viruses that behave more similarly to those that cause disease in humans. Continuing to passage virus in this manner will likely provide additional insights into DENV infection and mechanisms of disease, and viruses that cause disease in less immunocompromised mice at more physiologically relevant doses will be critical tools for development of DENV-specific therapies and treatments.

ACKNOWLEDGMENTS

This research was supported by a K22 grant (AI060989; NIAID) and a developmental project award from the Pacific Southwest Regional Center of Excellence (U54 AI065359; NIAID) to S.S.

We thank Eva Harris and Anna-Marija Helt at the University of California, Berkeley; Sondra Schlesinger, Milton Schlesinger, and Michael Diamond at Washington University School of Medicine, St. Louis, MO; and Chris Benedict, Shane Crotty, and members of the Shresta laboratory (Stuart Perry and Lauren Yauch) at LIAI for critical discussions and insights. We thank Dirk Zajonc at LIAI for assistance with the FPLC experiments. We thank Sarala Joshi, Steven Lada, Burton Barnett, and Afrina Qutubuddin for technical help.

REFERENCES

1. **An, J., J. Kimura-Kuroda, Y. Hirabayashi, and K. Yasui.** 1999. Development of a novel mouse model for dengue virus infection. Virology **263:**70–77.
2. **Bente, D. A., M. W. Melkus, J. V. Garcia, and R. Rico-Hesse.** 2005. Dengue fever in humanized NOD/SCID mice. J. Virol. **79:**13797–13799.
3. **Bernard, K. A., W. B. Klimstra, and R. E. Johnston.** 2000. Mutations in the E2 glycoprotein of Venezuelan equine encephalitis virus confer heparan sulfate interaction, low morbidity, and rapid clearance from blood of mice. Virology **276:**93–103.
4. **Blaney, J. E., Jr., A. P. Durbin, B. R. Murphy, and S. S. Whitehead.** 2006. Development of a live attenuated dengue virus vaccine using reverse genetics. Viral Immunol. **19:**10–32.
5. **Burke, D., and T. Monath.** 2001. Flaviviruses, p. 1043–1126. *In* D. Knipe and P. Howley (ed.), Field's virology. Lippincott/The Williams & Wilkins Co., Philadelphia, PA.
6. **Byrnes, A. P., and D. E. Griffin.** 1998. Binding of Sindbis virus to cell surface heparan sulfate. J. Virol. **72:**7349–7356.
7. **Byrnes, A. P., and D. E. Griffin.** 2000. Large-plaque mutants of Sindbis virus show reduced binding to heparan sulfate, heightened viremia, and slower clearance from the circulation. J. Virol. **74:**644–651.
8. **Couvelard, A., P. Marianneau, C. Bedel, M. Drouet, F. Vachon, D. Henin, and V. Deubel.** 1999. Report of a fatal case of dengue infection with hepatitis: demonstration of dengue antigens in hepatocytes and liver apoptosis. Hum. Pathol. **30:**1106–1110.
9. **Dasaneyavaja, A., and U. Charansri.** 1961. First known isolation of a dengue virus from other human source than blood, p. 61. SEATO Medical Research Monograph No. 2: Proceedings of the Symposium on Thai Hemorrhagic Fever, Bangkok, Thailand.
10. **Davis, C. W., H. Y. Nguyen, S. L. Hanna, M. D. Sanchez, R. W. Doms, and T. C. Pierson.** 2006. West Nile virus discriminates between DC-SIGN and DC-SIGNR for cellular attachment and infection. J. Virol. **80:**1290–1301.
11. **dos Santos, F. B., M. P. Miagostovich, R. M. Nogueira, H. G. Schatzmayr, L. W. Riley, and E. Harris.** 2004. Analysis of recombinant dengue virus polypeptides for dengue diagnosis and evaluation of the humoral immune response. Am. J. Trop. Med. Hyg. **71:**144–152.
12. **Falgout, B., M. Bray, J. J. Schlesinger, and C. J. Lai.** 1990. Immunization of mice with recombinant vaccinia virus expressing authentic dengue virus nonstructural protein NS1 protects against lethal dengue virus encephalitis. J. Virol. **64:**4356–4363.
13. **Green, S., D. W. Vaughn, S. Kalayanarooj, S. Nimmannitya, S. Suntayakorn, A. Nisalak, R. Lew, B. L. Innis, I. Kurane, A. L. Rothman, and F. A. Ennis.** 1999. Early immune activation in acute dengue illness is related to development of plasma leakage and disease severity. J. Infect. Dis. **179:**755–762.
14. **Gubler, D. J.** 1998. Dengue and dengue hemorrhagic fever. Clin. Microbiol. Rev. **11:**480–496.
15. **Hall, W., T. Crowell, D. Watts, V. Barros, H. Kruger, F. Pinheiro, and C. Peters.** 1991. Demonstration of yellow fever and dengue antigens in formalin-fixed paraffin-embedded human liver by immunohistochemical analysis. Am. J. Trop. Med. Hyg. **45:**408–417.
16. **Halstead, S. B.** 2007. Dengue. Lancet **370:**1644–1652.
17. **Helt, A. M., and E. Harris.** 2005. S-phase-dependent enhancement of dengue virus 2 replication in mosquito cells, but not in human cells. J. Virol. **79:**13218–13230.
18. **Hober, D., L. Poli, B. Roblin, P. Gestas, E. Chungue, G. Granic, P. Imbert, J. L. Pecarere, R. Vergez-Pascal, P. Wattre, et al.** 1993. Serum levels of tumor necrosis factor-α(TNF-α), interleukin-6 (IL-6), and interleukin-1β (IL-1β) in dengue-infected patients. Am. J. Trop. Med. Hyg. **48:**324–331.
19. **Houng, H. H., D. Hritz, and N. Kanesa-thasan.** 2000. Quantitative detection of dengue 2 virus using fluorogenic RT-PCR based on 3′-noncoding sequence. J. Virol. Methods **86:**1–11.
20. **Huang, K.-J., S.-Y. J. Li, S.-C. Chen, H.-S. Liu, Y.-S. Lin, T.-M. Yeh, C.-C. Liu, and H.-Y. Lei.** 2000. Manifestation of thrombocytopenia in dengue-2-virus-infected mice. J. Gen. Virol. **81:**2177–2182.
21. **Huerre, M., T. Nguyen, P. Marianneau, B. Nguyen, K. Huot, T. Nguyen, T. Nguyen, M. Drouet, T. Vu, Q. Do, Y. Buisson, and V. Deubel.** 2001. Liver histopathology and biological correlates in five cases of fatal dengue fever in Vietnamese children. Virchows Arch. **438:**107–115.
22. **Hung, S. L., P. L. Lee, H. W. Chen, L. K. Chen, C. L. Kao, and C. C. King.** 1999. Analysis of the steps involved in Dengue virus entry into host cells. Virology **257:**156–167.
23. **Jahrling, P. B., and L. Gorelkin.** 1975. Selective clearance of a benign clone of Venezuelan equine encephalitis virus from hamster plasma by hepatic reticuloendothelial cells. J. Infect. Dis. **132:**667–676.
24. **Jessie, K., M. Fong, S. Devi, S. Lam, and K. Wong.** 2004. Localization of dengue virus in naturally infected human tissues, by immunohistochemistry and in situ hybridization. J. Infect. Dis. **189:**1411–1418.
25. **Jinno-Oue, A., M. Oue, and S. K. Ruscetti.** 2001. A unique heparin-binding domain in the envelope protein of the neuropathogenic PVC-211 murine leukemia virus may contribute to its brain capillary endothelial cell tropism. J. Virol. **75:**12439–12445.
26. **Johnson, A. J., and J. T. Roehrig.** 1999. New mouse model for dengue virus vaccine testing. J. Virol. **73:**783–786.
27. **Kinney, R. M., S. Butrapet, G. J. Chang, K. R. Tsuchiya, J. T. Roehrig, N. Bhamarapravati, and D. J. Gubler.** 1997. Construction of infectious cDNA clones for dengue 2 virus strain 16681 and its attenuated vaccine derivative, strain PDK-53. Virology **230:**300–308.
28. **Kittigul, L., W. Temprom, D. Sujirarat, and C. Kittigul.** 2000. Determination of tumor necrosis factor-alpha levels in dengue virus-infected patients by sensitive biotin-streptavidin enzyme-linked immunosorbent assay. J. Virol. Methods **90:**51–57.
29. **Klimstra, W. B., K. D. Ryman, K. A. Bernard, K. B. Nguyen, C. A. Biron, and R. E. Johnston.** 1999. Infection of neonatal mice with Sindbis virus results in a systemic inflammatory response syndrome. J. Virol. **73:**10387–10398.
30. **Klimstra, W. B., K. D. Ryman, and R. E. Johnston.** 1998. Adaptation of Sindbis virus to BHK cells selects for use of heparan sulfate as an attachment receptor. J. Virol. **72:**7357–7366.
31. **Kuruvilla, J. G., R. M. Troyer, S. Devi, and R. Akkina.** 2007. Dengue virus infection and immune response in humanized RAG2$^{-/-}$ γc$^{-/-}$ (RAG-hu) mice. Virology **369:**143–152.
32. **Lee, E., R. A. Hall, and M. Lobigs.** 2004. Common E protein determinants for attenuation of glycosaminoglycan-binding variants of Japanese encephalitis and West Nile viruses. J. Virol. **78:**8271–8280.
33. **Lee, E., and M. Lobigs.** 2002. Mechanism of virulence attenuation of glycosaminoglycan-binding variants of Japanese encephalitis virus and Murray Valley encephalitis virus. J. Virol. **76:**4901–4911.
34. **Lee, E., P. J. Wright, A. Davidson, and M. Lobigs.** 2006. Virulence attenu-

ation of Dengue virus due to augmented glycosaminoglycan-binding affinity and restriction in extraneural dissemination. J. Gen. Virol. **87:**2791–2801.
35. **Libraty, D. H., T. P. Endy, H. S. Houng, S. Green, S. Kalayanarooj, S. Suntayakorn, W. Chansiriwongs, D. W. Vaughn, A. Nisalak, F. A. Ennis, and A. L. Rothman.** 2002. Differing influences of virus burden and immune activation on disease severity in secondary dengue-3 virus infections. J. Infect. Dis. **185:**1213–1221.
36. **Lin, Y. L., C. L. Liao, L. K. Chen, C. T. Yeh, C. I. Liu, S. H. Ma, Y. Y. Huang, Y. L. Huang, C. L. Kao, and C. C. King.** 1998. Study of Dengue virus infection in SCID mice engrafted with human K562 cells. J. Virol. **72:**9729–9737.
37. **Lyon, M., J. A. Deakin, and J. T. Gallagher.** 1994. Liver heparan sulfate structure: a novel molecular design. J. Biol. Chem. **269:**11208–11215.
38. **Miagostovich, M., R. Ramos, A. Nicol, R. Nogueira, T. Cuzzi-Maya, A. Oliveira, R. Marchevsky, R. Mesquita, and H. Schatzmayr.** 1997. Retrospective study on dengue fatal cases. Clin. Neuropathol. **16:**204–208.
39. **Modis, Y., S. Ogata, D. Clements, and S. C. Harrison.** 2003. A ligand-binding pocket in the dengue virus envelope glycoprotein. Proc. Natl. Acad. Sci. USA **100:**6986–6991.
40. **Modis, Y., S. Ogata, D. Clements, and S. C. Harrison.** 2005. Variable surface epitopes in the crystal structure of dengue virus type 3 envelope glycoprotein. J. Virol. **79:**1223–1231.
41. **Mukhopadhyay, S., R. J. Kuhn, and M. G. Rossmann.** 2005. A structural perspective of the flavivirus life cycle. Nat. Rev. Microbiol. **3:**13–22.
42. **Navarro-Sanchez, E., R. Altmeyer, A. Amara, O. Schwartz, F. Fieschi, J. L. Virelizier, F. Arenzana-Seisdedos, and P. Despres.** 2003. Dendritic-cell-specific ICAM3-grabbing non-integrin is essential for the productive infection of human dendritic cells by mosquito-cell-derived dengue viruses. EMBO Rep. **4:**1–6.
43. **Nisalak, A., S. Halstead, P. Singharaj, S. Udomsakdi, S. Nye, and K. Vinijchaikul.** 1970. Observations related to pathogenesis of dengue hemorrhagic fever. III. Virologic studies of fatal disease. Yale J. Biol. Med. **42:**293–310.
44. **Ramos, C., G. Sanchez, R. Pando, J. Baquera, D. Hernandez, J. Mota, J. Ramos, A. Flores, and E. Llausas.** 1998. Dengue virus in the brain of a fatal case of hemorrhagic dengue fever. J. Neurovirol. **4:**465–468.
45. **Reddi, H. V., and H. L. Lipton.** 2002. Heparan sulfate mediates infection of high-neurovirulence Theiler's viruses. J. Virol. **76:**8400–8407.
46. **Rosen, L., M. Drouet, and V. Deubel.** 1999. Detection of dengue virus RNA by reverse transcription-polymerase chain reaction in the liver and lymphoid organs but not in the brain in fatal human infection. Am. J. Trop. Med. Hyg. **61:**720–724.
47. **Ryman, K. D., C. L. Gardner, C. W. Burke, K. C. Meier, J. M. Thompson, and W. B. Klimstra.** 2007. Heparan sulfate binding can contribute to the neurovirulence of neuroadapted and nonneuroadapted Sindbis viruses. J. Virol. **81:**3563–3573.
48. **Ryman, K. D., W. B. Klimstra, K. B. Nguyen, C. A. Biron, and R. E. Johnston.** 2000. Alpha/beta interferon protects adult mice from fatal Sindbis virus infection and is an important determinant of cell and tissue tropism. J. Virol. **74:**3366–3378.
49. **Sa-Carvalho, D., E. Rieder, B. Baxt, R. Rodarte, A. Tanuri, and P. W. Mason.** 1997. Tissue culture adaptation of foot-and-mouth disease virus selects viruses that bind to heparin and are attenuated in cattle. J. Virol. **71:**5115–5123.
50. **Scherer, W. F., R. W. Dickerman, and J. V. Ordonez.** 1977. Serologic surveys for antibodies to Western, Eastern, California, and St. Louis encephalitis and Dengue 3 arboviruses in Middle America, 1961–1975. Bull. Pan Am. Health Org. **11:**212–223.
51. **Shresta, S., J. L. Kyle, P. Robert Beatty, and E. Harris.** 2004. Early activation of natural killer and B cells in response to primary dengue virus infection in A/J. mice. Virology **319:**262–273.
52. **Shresta, S., J. L. Kyle, H. M. Snider, M. Basavapatna, P. R. Beatty, and E. Harris.** 2004. Interferon-dependent immunity is essential for resistance to primary dengue virus infection in mice, whereas T- and B-cell-dependent immunity are less critical. J. Virol. **78:**2701–2710.
53. **Shresta, S., K. L. Sharar, D. M. Prigozhin, P. R. Beatty, and E. Harris.** 2006. Murine model for dengue virus-induced lethal disease with increased vascular permeability. J. Virol. **80:**10208–10217.
54. **Tassaneetrithep, B., T. H. Burgess, A. Granelli-Piperno, C. Trumpfheller, J. Finke, W. Sun, M. A. Eller, K. Pattanapanyasat, S. Sarasombath, D. L. Birx, R. M. Steinman, S. Schlesinger, and M. A. Marovich.** 2003. DC-SIGN (CD209) mediates dengue virus infection of human dendritic cells. J. Exp. Med. **197:**823–829.
55. **Van Gennip, H. G., A. C. Vlot, M. M. Hulst, A. J. De Smit, and R. J. Moormann.** 2004. Determinants of virulence of classical swine fever virus strain Brescia. J. Virol. **78:**8812–8823.
56. **Vaughn, D. W., S. Green, S. Kalayanarooj, B. L. Innis, S. Nimmannitya, S. Suntayakorn, T. Endy, B. Raengsakulrach, A. L. Rothman, F. A. Ennis, and A. Nisalak.** 2000. Dengue viremia titer, antibody response pattern, and virus serotype correlate with disease severity. J. Infect. Dis. **181:**2–9.
57. **Wang, W. K., D. Y. Chao, C. L. Kao, H. C. Wu, Y. C. Liu, C. M. Li, S. C. Lin, S. T. Ho, J. H. Huang, and C. C. King.** 2003. High levels of plasma dengue viral load during defervescence in patients with dengue hemorrhagic fever: implications for pathogenesis. Virology **305:**330–338.
58. **Wu, S. J., C. G. Hayes, D. R. Dubois, M. G. Windheuser, Y. H. Kang, D. M. Watts, and D. G. Sieckmann.** 1995. Evaluation of the severe combined immunodeficient (SCID) mouse as an animal model for dengue viral infection. Am. J. Trop. Med. Hyg. **52:**468–476.